ASSOCIAZIONE NAZIONALE ITALIANA DI INGEGNERIA SISMICA
ANIDIS
Italian National Association of Earthquake Engineering

XVIII CONVEGNO ANIDIS
L'ingegneria sismica in Italia
ASCOLI PICENO 2019
15-19 Settembre

Effectiveness of FRCM systems in confining concrete members: analytical models

Annalisa Napoli[a], Roberto Realfonzo[a]
[a] *Dipartimento di Ingegneria Civile, Università degli Studi di Salerno, Via Giovanni Paolo II, 132, 84084 Fisciano (SA), Italy*

Keywords: Analytical investigation; concrete; confinement; FRCM system; strength

ABSTRACT
Composite materials employing cement-based mortars, usually known as fabric-reinforced cementitious matrix (FRCM) composites, have recently emerged as a promising, sustainable, and durable solution for the repairing and strengthening of reinforced concrete or masonry members. They represent an attractive alternative to the use of Fiber Reinforced Polymer (FRP) composites when there is a need to overcome some of the disadvantages related to the epoxy resin, such as moderate matrix heat and fire resistance, difficulty of application at low temperatures, impossibility of application on wet surfaces, and lack of vapor permeability. This paper presents an analytical study on the confinement of concrete columns with FRCM composites. To this purpose, a wide database including results of compression tests performed on over 290 concrete cylinders externally wrapped with FRCM was assembled from the literature. The collected results were employed to perform an overall analysis of the efficiency of the FRCM confinement by varying some of the relevant parameters, such as: type of fiber (glass, carbon, steel, PBO or basalt) and geometry of the mesh, number of employed layers, mechanical properties of the inorganic matrix and compressive strength of the unconfined concrete. Relationships for estimating the compression strength of the FRCM confined concrete were then developed through best-fit analyses, and comparisons with some formulations available in the literature were performed.

1 INTRODUCTION AND BACKGROUND

In existing reinforced concrete (RC) framed buildings, the external confinement of deficient columns with Fiber Reinforced Polymers (FRPs) represents today a competitive alternative to the use of traditional techniques such as steel or concrete jacketing. However, drawbacks related to the epoxy resin cannot be ignored and include moderate matrix heat and fire resistance, low glass transition temperature, difficulty of application at low temperatures, impossibility of application on wet surfaces, and lack of vapor permeability.

In order to overcome these issues, composite materials employing inorganic matrices, mainly made of cement-based mortars, have recently been proposed as a "green" solution which can be an attractive alternative to FRPs.

These composites are generally called Fabric-Reinforced Cementitious Matrix (FRCM), although several other names are used in the literature based on the type of matrix, application, and substrate to strengthen, i.e., concrete or masonry (D'Ambrisi et al. 2013).

The most commonly-used fibers are made of basalt (B), carbon (C), alkali-resistant (AR) glass (G), poliparafenilenbenzobisoxazole (PBO) and steel (S). These fibers are typically arranged in bundles and their configuration can be modified from unidirectional to bidirectional textile weaves or fabrics in an attempt to improve bond properties. The spacing among the bundles facilitates the impregnation of each bundle and assures matrix continuity among internal and external matrix layers.

Regarding the steel fibers, it has to be highlighted that they are improperly called "fibers" being actually composed of ultra-high tensile strength steel (UHTSS) micro-wires, which are twisted around each other to form cords or ropes with a micro-fine brass or galvanized coating. Also in this case, the cord spacing is very important to assure a proper matrix impregnation, so that different tape densities are now commercially available.

The research studies available on the effectiveness of FRCM systems for RC

strengthening applications are rather limited if compared to FRPs, also due to their relatively recent market entry. However, also thanks to the increased sensitivity by industry and scientific community towards sustainability issues, a number of experimental and theoretical researches have been performed in the last ten years; state-of-the-art reports have been authored by Carloni et al. (2016, 2018).

Some attempts towards a design approach for the FRCM systems were also made in these last years, in particular:

- in 2013, with the publication of the guide ACI 549.4R (2013), in which all commonly-used fibers were included, i.e., AR glass, carbon, basalt and PBO, except steel fibers and pre-impregnated fabrics;
- in 2018, with the publication of the document CNR-DT 215 (2018) which represents the first effort in Italy to organize in a systematic framework the existing knowledge on FRCM composites and promulgate some basic principles of the strengthening design.

Experimental studies show that the mechanical behavior of FRPs and FRCMs is significantly different under tensile loading, since the strength of FRCM systems is affected by the type and size of the adopted fibers, by the mesh layout and by the properties of the matrix (Ascione et al. 2015). At the same way, concrete columns confined with FRP and FRCM systems show a significantly different behavior under compression loads as described in Faella et al. (2018).

The stress-strain behavior of FRCM-confined specimens relies on many factors depending on both the type of FRCM system and the wet lay-up installation procedure. A key factor influencing the stress-strain response is of course the quality of the mortar and the corresponding bond at the fiber-matrix interface; the cracking of the mortar, often occurring prematurely (when its mechanical properties are very poor) is generally responsible for the post-peak softening behavior.

Based on the above considerations, developing accurate models for estimating the compressive strength and ultimate strain of the FRCM-confined concrete is an open issue since the greater or lesser influence of all the mentioned physical and behavioral aspects depends on the specific FRCM confining system.

Some formulations have been recently proposed by Ombres and Mazzuca (2017), Cascardi et al. (2017) and, lately, by the above mentioned document CNR-DT 215 (2018).

The paper provides a further contribute in this sense by proposing new models for the estimate of the compressive strength of the FRCM confined concrete. An updated database including 293 concrete cylinders externally wrapped with different FRCM systems was got from the literature. The strength models were developed through best-fit techniques applied to the experimental data. Comparisons with other formulations available in the literature for either FRP or FRCM composites were also made.

2 EXPERIMENTAL DATABASE

The assembled databased includes the results of 293 compression tests performed on plain concrete cylinders confined with different FRCM systems. Among the specimens, 68 were confined with B-FRCM, 50 with C-FRCM, 53 with G-FRCM, 42 with PBO-FRCM and 80 with S-FRCM systems. The pie chart in Figure 1 illustrates the percentage (%) distribution per FRCM system of the 293 specimens included in the database.

The specimens had diameter to-height (H/D) ratio comprised approximately between 2 and 3, and were manufactured with concrete mixtures characterized by an average value of the cylindrical compressive strength (f_{c0}) in the range 11-52 MPa.

Both unidirectional (UD) and bidirectional (BD) fabrics were used for concrete confinement. Several fiber amounts were adopted in the manufacture of the fabrics in order to have various dry textile's equivalent thicknesses (t_f).

Different inorganic matrices - from pozzolanic to hydraulic ones - were used to impregnate the fabric and their mechanical properties were rather dispersed.

In all the cases, the concrete cylinders were wrapped with fabric meshes by using a number of layers (n_f) ranging between 1 and 6; the angle of fiber inclination with respect to the longitudinal axis (θ) of the specimen was 90°, except in some PBO-FRCM confined specimens where the inclination was 30° and 45°.

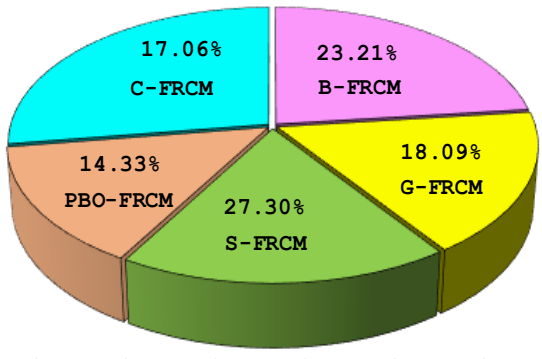

Figure 1. % distribution per FRCM system of specimens included in the database.

Table 1. Range of variation of the main parameters considered in the database.

System / *Parameter*	B-FRCM	C-FRCM	G-FRCM	PBO-FRCM	S-FRCM
D [mm]	110-150	140-200	150	113-200	150
H/D [-]	2.0	2.0-3.3	2.0	1.9-3.3	2.0
f_{c0} [MPa]	15.52-32.20	11.40-36.80	15.52-38.41	11.40-52.39	15.12-29.98
$f_{m,c}$ [MPa]	22.40-82.00	17.00-82.00	2.50-82.00	30.4-50.0	4.1-55.0
$f_{m,b}$ [MPa]	4.10-9.00	3.60-9.50	0.20-9.00	2.00-6.20	1.00-10.00
E_m [GPa]	-	12.5-34.5	-	6.1-34.5	8.0-25.0
t_m [mm]	10.0-15.0	4.0-12	6.0-20.0	6.0-20.0	7.0-10.0
Type [-]	BD	UD-BD	UD-BD	UD-BD	UD
t_f [mm]	0.046-0.200	0.047-0.168	0.043-0.600	0.046	0.062-0.562
$f_{f,u}$ [MPa]	658.7-2800	1032-4800	451-4200	5800	1870-2800
E_{fn} [GPa]	52.00-93.00	204.00-330.00	71.00-76.90	270.00	110.00-190.00
$\varepsilon_{f,u}$ [%]	2.00-2.80	0.46-2.00	1.65-5.60	2.00-2.50	1.50-2.10
n_f	1-2	1-3	1-6	1-4	1-2
θ [°]	90	90	90	30-90	90
f_l/f_{c0}	0.01-0.51	0.07-0.97	0.05-2.75	0.07-1.05	0.07-1.29
k_ε	0.20-0.35	-	0.08-0.44	0.21-0.83	-

Table 1 provides, for each type of FRCM system, all the ranges of variation of the main parameters considered in the database, in particular: *a)* specimen's diameter and H/D ratio; *b)* f_{c0} as defined earlier; *c)* mechanical properties of the inorganic matrix (when available), i.e., compressive strength ($f_{m,c}$), flexural strength ($f_{m,b}$) and modulus of elasticity (E_m); *d)* total thickness of the mortar layer used for fabric's application (t_m); *e)* fabric geometry (UD/BD), equivalent thickness (t_f) of the single layer of the dry fabric and corresponding mechanical properties, i.e., elastic modulus (E_f), ultimate tensile strength ($f_{f,u}$) and corresponding strain ($\varepsilon_{f,u}$); *f)* n_f and θ as defined earlier; *g)* lateral confining pressure exerted by the FRCM jacket, normalized with respect to the concrete strength ($\bar{f}_l = f_l/f_{c0}$) and strain efficiency factor of the FRCM system (k_ε) defined, similarly to FRPs, as the ratio between the ultimate hoop strain reached in the FRCM jacket ($\varepsilon_{j,u}$) and the ultimate strain found from flat coupon tensile tests ($\varepsilon_{f,u}$).

It is mentioned that the values of $\bar{f}_l$ in Table 1 refer to the ultimate lateral confining pressure of the FRCM jacket since they were calculated by plugging $k_\varepsilon = 1$ in the following relationship:

$$\bar{f}_l = \frac{f_l}{f_{c0}} = k_\alpha \cdot \frac{2 \cdot t_f \cdot n_f \cdot E_f}{D} \cdot (k_\varepsilon \cdot \varepsilon_{f,u}) \quad (1)$$

where k_α is the coefficient accounting for the fiber inclination, equal to 1 in the case of θ=90°, which was calculated according to CNR-DT200 R1 (2013):

$$k_\alpha = \frac{1}{1+[tan(90°-\theta)]^2} \quad (2)$$

It is worth mentioning that, as already done in a previous investigation carried out by Realfonzo and Napoli (2011), the analytical study presented in the next section was performed by considering a smaller database, where all the experimental data and results were collected in 130 homogeneous datasets. Each set represents a group of *N* experimental tests characterized by uniformity in terms of: *a)* specimen size (D, H); *b)* compressive strength f_{c0}, *c)* geometry (UD/BD, density, t_f, n_f, θ), and mechanical properties of the dry fabric, i.e., E_f, $f_{f,u}$ and $\varepsilon_{f,u}$, *d)* mechanical properties of the inorganic matrix $f_{m,c}$, $f_{m,b}$ and E_m, and *e)* observed failure mode. The experimental results attributed to each dataset represent, therefore, the average values obtained for the collected *N* tests.

The pie chart in Figure 2 illustrates the % distribution per FRCM system of the 130 datasets extracted from the general database. In particular, the number n of datasets was equal to 18, 23, 20, 31 and 38 for B-, C-, G-, PBO- and S-FRCM system, respectively.

The resulting database is reported in Table 2 and represents an update of that reported in a preliminary study (Faella et al. 2018).

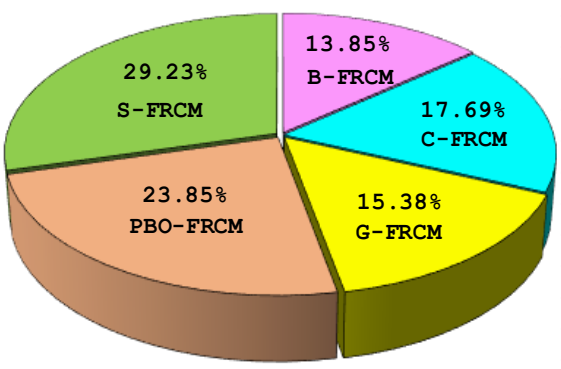

Figure 2. % distribution of datasets per FRCM system within the database.

Table 2. Experimental database.

Source	Specimen label	N	Geometry		Matrix's properties				Fabric mesh's properties						Jacket		Results				
			D	H/D	$f_{m,c}$	$f_{m,b}$	E_m	t_m	*type*	*density*	t_f	$f_{f,u}$	E_f	$\varepsilon_{f,u}$	n_f	θ	f_l/f_{c0}	f_{c0}	f_{cc}	k_ε	FM
			[mm]	[-]	[MPa]	[MPa]	[GPa]	[mm]	[-]	[g/m^2]	[mm]	[MPa]	[GPa]	[%]	[-]	[°]	[-]	[MPa]	[MPa]	[-]	
B-FRCM system																					
[1]	S4-S6	2	150	2.0	30.00	9.00	–	10	BD*	254	0.046	1814	91.10	2.0	1	90	0.07	15.52	21.11	0.20	JF
	S5-S7	2	150	2.0				15							2		0.14		22.66	0.35	JF
	S14-S15-S18-S19	4	150	2.0				10	BD**						1		0.06	17.83	24.12	0.22	JF
	S16-S17-S20-S21	4	150	2.0				15							2		0.13		27.55	0.30	JF
[2]	M1-1,..6	6	150	2.0	31.50	4.10	–	10	BD	238	0.086	894	52.00	2.2	1	90	0.06	21.80	26.20	–	JF
	M2-1,..6	6	150	2.0				15							2		0.12		27.21	–	JF
	C1-1,..6	6	150	2.0	22.40	4.70	–	10							1		1.31		28.67	–	JF
	C2-1,..6	6	150	2.0				15							2		0.06		28.78	–	JF
[3]	B-CM-1	4	150	2.0	82.00	–	–	–	UD	220	0.200	2800	93.00	2.8	1	90	0.25	27.30	32.00	–	JF
	B-CM-2	4	150	2.0											2		0.51		35.00	–	JF
[4]	C-ECC-TB (1)	3	110	2.0	65.00	–	–	–	BD	120	–	658.7	–	–	1	90	0.09	15.80	21.95	0.83	JF
	C-ECC-TB-O (1)	3	110	2.0											1		0.09		20.77	0.70	JF
	C-ECC-TB-OS (1)	3	110	2.0											1		0.09		21.20	0.91	JF
	C-M-TB (1)	3	110	2.0	46.00	–	–	–							1		0.02		19.00	0.42	JF
	C-ECC-TB (2)	3	110	2.0	65.00	–	–	–							1		0.04	32.20	38.75	1.20	JF
	C-ECC-TB-O (2)	3	110	2.0											1		0.04		37.14	1.22	JF
	C-ECC-TB-OS (2)	3	110	2.0											1		0.04		37.75	1.51	JF
	C-M-TB (2)	3	110	2.0	46.00	–	–	–							1		0.01		35.31	1.09	JF
C-FRCM system																					
[5]	A_MI2	3	150	2.0	8.56	3.28	14.63	6	BD	168	0.047	3350	225.00	1.49	2	90	0.28	15.24	20.77	–	*D*
	A_MII2	3	150	2.0	30.61	4.24	27.66	6							2		0.28		23.88	–	JF
	A_MI3	3	150	2.0	8.56	3.28	14.63	8							3		0.41		26.50	–	*D*
	A_MII3	3	150	2.0	30.61	4.24	27.66	8							3		0.41		27.00	–	JF
	B_MII2	3	150	2.0	30.61	4.24	27.66	6							2		0.19	21.81	27.36	–	JF
	B_MII3	3	150	2.0	30.61	4.24	27.66	8							3		0.29		32.44	–	JF
[6]	SERIES C	2	150	2.0	67.00	–	–	–	BD	111	–	1032	222.98	0.46	2	90	–	26.00	39.00	–	*D*
	SERIES D	2	150	2.0						324	–	–	204.00	–	3		–		57.00	–	*D*
[7]	CF2M-a	1	200	3.0	31.17	9.50	>15.00	9	BD	168	0.047	4800	240.00	2.0	2	90	0.27	16.80	20.83	–	JF
	CF2M-b	1	200	3.0				9							2		0.28	16.08	20.58	–	JF
	CF3M-a	1	200	3.0				12							3		0.40	16.80	23.69	–	JF
	CF3M-b	1	200	3.0				12							3		0.42	16.08	23.96	–	JF
[3]	C-CM-1	4	150	2.0	82.00	–	–	–	UD	245	0.168	3900	330.00	1.80	1	90	0.49	27.30	35.00	–	*D*
	C-CM-2	4	150	2.0											2		0.97		42.00	–	JF
[8]	C1-gro2-Y-a,b	2	150	2.0	–	–	–	6	UD	300	0.167	4093	244.00	1.72	1	90	0.27	34.62	43.82	–	JF
	C1-gro3-Y-a,b	2	150	2.0				6							1		0.27		43.04	–	JF
	C2-gro3-Y-a,b	2	150	2.0				9							2		0.54		57.60	–	JF
[9]	CCML1D0-1,..3	3	150	2.0	25.00	–	–	4-8	BD	170	0.047	4700	240.00	1.80	1	90	0.07	36.80	38.80	–	*D*
[10]	M15_CF_1	1	140	3.3	17.00	3.60	12.50	8	BD	172	0.048	4800	235.00	1.50	1	90	0.21	11.40	13.32	–	JF
	M15_CF_2	1	140	3.3				12							2		0.42		13.98	–	JF
	M45_CF_1	1	140	3.3	50.00	6.20	34.50	8							1		0.21		13.85	–	JF
	M45_CF_2	1	140	3.3				12							2		0.42		13.46	–	JF
[11]	C-S3-D0-1,2,3	3	150	2.0	22.80	5.23	–	–	BD	2200	0.047	4700	240.00	1.80	2	90	5.41	16.80	22.18	–	JF
G-FRCM system																					
[1]	S3	1	150	2.0	30.00	9.00	–	12	BD	225	0.043	1440	72.00	2.00	2	90	0.11	15.52	22.35	0.44	JF
	S10,..S12	3	150	2.0				8							1		0.05	17.83	20.03	0.22	JF
	S13	1	150	2.0				12							2		0.09		23.00	0.36	JF
[12]	FABcrete	4	150	2.0	56.26	6.25	–	–	BD***	225	–	45[1]	–	>3.00	–	–	–	38.41	41.28	–	*D*
[6]	SERIE B	2	150	2.0	67.00	–	–	–	BD	167[2]		1231	74.45	1.65	6	90	–	26.00	35.00	–	*D*
[13]	LDG-A-1, A-2	2	152	2.0	2.49	0.20	–	12	UD	525	0.217	3240	72.40	4.50	2	90	0.91	20.40	26.85	–	*D*
	LDG-H-1, H-2	2	152	2.0	31.10	1.36	–	12							2		0.91		30.00	–	*D*
	HDG-A-1, A-2	2	152	2.0	2.49	0.20	–	12		915	0.378	3240	72.40	4.50	2		1.59		24.50	–	*D*
	HDG-H-1, H-2	2	152	2.0	31.10	1.36	–	12							2		1.59		30.00	–	*D*
	1B-1,…3	3	152	2.0	31.10	1.36	–	8		596	0.246	3399	76.90	4.40	1		0.50	21.70	26.30	0.08	*D*
	2B-1,…6	6	152	2.0				12							2		1.01		35.52	0.11	*D*
	2U-1,…6[4]	6	152	2.0				12							2		1.01		33.93	0.08	*D*
	4B-1,…3	3	152	2.0				20							4		2.02		47.90	0.22	*D*
[14]	CSW	1	150	2.0	–	–	–	–	BD	610	0.600	4200	75.00	5.60	1	90	1.38	24.41	33.60	–	JF
	CDW	1	150	2.0											2		2.75		51.16	–	JF
[3]	G-CM-1	4	150	2.0	82.00	–	–	–	UD	192	0.220	2100	71.00	2.60	1	90	0.20	27.30	31.00	–	JF
	G-CM-2	4	150	2.0											2		0.40		33.00	–	JF
[8]	G1-gro3-N-a,b	2	150	2.0	–	–	–	6	UD	450	0.177	1500	72.00	2.00	1	90	0.10	34.62	36.81	–	JF
	G1-gro3-Y-a,b	2	150	2.0				6							1		0.10		42.31	–	JF
	G2-gro3-Y-a,b	2	150	2.0				9							2		0.20		50.12	–	JF

Table 2. Experimental database. *(continued)*

Source	Specimen label	N	Geometry		Matrix's properties				Fabric mesh's properties						Jacket		Results				
			D	H/D	$f_{m,c}$	$f_{m,b}$	E_m	t_m	*type*	*density*	t_f	$f_{f,u}$	E_f	$\varepsilon_{f,u}$	n_f	θ	f_l/f_{c0}	f_{c0}	f_{cc}	k_ε	FM
			[mm]	[-]	[MPa]	[MPa]	[GPa]	[mm]	[-]	[g/m^2]	[mm]	[MPa]	[GPa]	[%]	[-]	[°]	[-]	[MPa]	[MPa]	[-]	
PBO-FRCM system																					
[7]	CA1,..3-2L	3	154	2.2	≥ 15.00	≥ 2.00	≥ 6.10	9-12	BD	88	0.045	5800	270.00	2.15	2	90	0.28	24.20	31.23	0.43	JF
	CA4, 6-3L	3	154	2.2				12-16							3		0.42		36.57	0.51	JF
	CB2,4,6-2L	3	200	1.7				9-12							2		0.21	24.40	31.17	0.72	JF
	CB1,5-3L	2	200	1.7				12-16							3		0.32		33.55	0.81	JF
[14]	20M1_1,2	2	113	2.7	29.0	3.50	6.00	10	BD	88	0.0455	5800	270.00	2.15	1	90	0.21	22.60	32.57	0.34	*D*
	20M2_1,2	2	113	2.7				15							2		0.41		42.69	0.34	*D*
	20M3_1,2	2	113	2.7				20							3		0.62		56.94	0.34	*D*
[15]	CRP1-I	1	152	1.9	30.40	–	6.10	6	BD	–	0.0455	5800	270.00	2.00	1	90	0.21	15.40	24.69	0.42	JF
	CRP2-I	1	152	1.9				9							2		0.42		35.00	0.47	JF
	CRP3-I	1	152	1.9				12							3		0.79		41.45	0.52	JF
	CRP4-I	1	152	1.9				15							4		1.05		49.24	0.41	JF
	CRP5-I	1	152	1.9				6							1	45	0.16		16.19	0.40	JF
	CRP6-I	1	152	1.9				9							2		0.31		16.98	0.40	JF
	CRP7-I	1	152	1.9				12							3		0.47		17.40	0.50	JF
	CRP8-I	1	152	1.9				9							2	30	0.26		17.45	0.64	JF
	CRP9-I	1	152	1.9				12							3		0.39		21.69	0.50	JF
	CRP1-II	1	153	1.9				6							1	90	0.11		43.55	0.30	*D*
	CRP2-II	1	153	1.9				9							2		0.22		47.00	0.52	*D*
	CRP3-II	1	153	1.9				12							3		0.33		56.60	0.53	*D*
	CRP4-II	1	153	1.9				15							4		0.44		56.23	0.83	*D*
	CRP5-II	1	152	1.9				6							1	45	0.08	29.26	31.68	0.34	JF
	CRP6-II	1	152	1.9				9							2		0.16		33.79	0.51	JF
	CRP7-II	1	152	1.9				12							3		0.25		35.72	0.56	JF
	CRP8-II	1	152	1.9				9							2	30	0.14		35.42	0.52	JF
	CRP9-II	1	152	1.9				12							3		0.21		39.52	0.49	JF
[16]	CI-1-20-1,2	2	151	2.0	30.40	–	6.14	6	BD	–	0.0455	5800	270.00	2.15	1	90	0.10	33.83	35.80	0.46	JF
	CIII-1-20	1	150	2.0				6							1		0.07		54.90	0.25	JF
	CIII-2-20	1	150	2.0				9							2		0.13	52.39	51.45	0.46	JF
	CIII-3-20	1	150	2.0				12							3		0.20		55.94	0.21	JF
[10]	M45_PBO_1	1	140	3.3	50.00	6.20	34.50	8	UD	146	0.046	5800	270.00	2.50	1	90	0.39	11.40	18.14	–	JF
	M45_PBO_2	1	140	3.3				12							2		0.78		17.27	–	JF
S-FRCM system																					
[17]	A3 x 2h1_1,2	2	150	2.0	22.10	6.78	8.03	10	UD	9.06[3]	0.562	2187	130.02	2.00	1	90	1.29	15.12	22.27	–	*D*
	A3 x 2m1_1,2	2	150	2.0				7		2.00[3]	0.124	2187	130.15	2.00	1		0.28		24.70	–	JF
	A3 x 2m1_3	1	150	2.0				7		2.00[3]	0.124	2187	130.15	2.00	1		0.28		27.58	–	*D*
	A3 x 2l1_1,..3	3	150	2.0				7		1.00[3]	0.062	2187	130.15	2.00	1		0.14		22.80	–	JF
	A12 x h1_1,2	2	150	2.0				10		9.06[3]	0.562	1870	130.02	1.60	1		1.03		25.30	–	*D*
	A12 x m1_1,3	2	150	2.0				7		2.00[3]	0.124	1870	130.15	1.60	1		0.23		26.24	–	*D*
	A12 x m1_2	1	150	2.0				7		2.00[3]	0.124	1870	130.15	1.60	1		0.23		27.46	–	JF
	A12 x l1_1,..3	3	150	2.0				7		1.00[3]	0.062	1870	130.15	1.60	1		0.11		22.55	–	JF
	B3 x 2m2_1,..3	3	150	2.0				7		2.00[3]	0.124	2187	130.15	2.00	1		0.16	26.20	36.07	–	*D*
	B3 x 2l2_1,2	2	150	2.0				7		1.00[3]	0.062	2187	130.15	2.00	1		0.08		35.97	–	*D*
	B3 x 2l2_3	1	150	2.0				7		1.00[3]	0.062	2187	130.15	2.00	1		0.08		35.84	–	JF
	B12 x m2_1,..3	3	150	2.0				7		2.00[3]	0.124	1870	130.15	1.60	1		0.13		40.42	–	*D*
	B12 x l2_1,3	2	150	2.0				7		1.00[3]	0.062	1870	130.15	1.60	1		0.07		35.37	–	JF
	B12 x l2_2	1	150	2.0				7		1.00[3]	0.062	1870	130.15	1.60	1		0.07		37.90	–	*D*
[18]	A1#1	1	150	2.0	22.10	6.78	8.03	7	UD	1.00[3]	0.062	2014	110.00	1.90	1	90	0.07	16.62	28.75	–	JF
	A2#1-1,2	2	150	2.0				7		1.00[3]	0.062	2480	120.00	2.10	1		0.09		32.30	–	JF
	A2#2-1,..3	3	150	2.0				10		1.00[3]	0.062	2480	120.00	2.10	2		0.18		38.56	–	JF
	A3#1	1	150	2.0	4.06	1.00	10.35	7		1.00[3]	0.062	2014	110.00	1.90	1		0.07	23.14	29.80	–	JF
	A4#1-1,2	2	150	2.0				7		1.00[3]	0.062	2480	120.00	2.10	1		0.09		30.12	–	JF
	A4#2-1,..3	3	150	2.0				10		1.00[3]	0.062	2480	120.00	2.10	2		0.18		34.02	–	JF
	A5#1	1	150	2.0	20.10	4.24	18.63	7		1.00[3]	0.062	2014	110.00	1.90	1		0.07		33.07	–	JF
	A6#1-1,2	2	150	2.0				7		1.00[3]	0.062	2480	120.00	2.10	1		0.09		32.15	–	JF
	A6#2-1,..3	3	150	2.0				10		1.00[3]	0.062	2480	120.00	2.10	2		0.18		38.02	–	JF
	B1#1	1	150	2.0	22.10	6.78	8.03	7		1.00[3]	0.062	2014	110.00	1.90	1		0.10		30.45	–	JF
	B3#1	1	150	2.0	4.06	1.00	10.35	7		1.00[3]	0.062	2014	110.00	1.90	1		0.10		26.64	–	JF
	B5#2	1	150	2.0	20.10	4.24	18.63	10		1.00[3]	0.062	2014	110.00	1.90	2		0.21		28.32	–	JF
	C7#1-1,..3	3	150	2.0	55.00	10.00	25.00	7		1.57[3]	0.084	2800	190.00	1.50	1		0.15	20.73	31.36	–	*D*
	C8#1-1,2	2	150	2.0				7		1.57[3]	0.084	2800	190.00	1.50	1		0.15		34.10	–	JF
	C7/8#2-1,2	4	150	2.0				10		1.57[3]	0.084	2800	190.00	1.50	2		0.31		42.44	–	JF
	D8#1-1	1	150	2.0				7		1.57[3]	0.084	2800	190.00	1.50	1		0.17	18.27	27.53	–	JF
	D8#1-2,3	2	150	2.0				7		1.57[3]	0.084	2800	190.00	1.50	1		0.17		27.75	–	*JF-D*
	D7#2-1,..3	3	150	2.0				10		1.57[3]	0.084	2800	190.00	1.50	2		0.35		36.44	–	JF
	D9#1-1,..3	3	150	2.0				7		4.72[3]	0.254	2800	190.00	1.50	1		0.53		40.64	–	*D*
	D10#2-1,2	2	150	2.0				10		4.72[3]	0.254	2800	190.00	1.50	2		1.06		53.53	–	*JF-D*
	E8#1-1,2	2	150	2.0				7		4.72[3]	0.254	2800	190.00	1.50	1		0.32	29.98	40.51	–	JF

Table 2. Experimental database. *(continued)*

S-FRCM system																					
Source	Specimen label	*N*	Geometry		Matrix's properties				Fabric mesh's properties						Jacket		Results				
			D	*H/D*	$f_{m,c}$	$f_{m,b}$	E_m	t_m	*type*	*density*	t_f	$f_{f,u}$	E_f	$\varepsilon_{f,u}$	n_f	θ	f_l/f_{c0}	f_{c0}	f_{cc}	k_ε	FM
			[mm]	[-]	[MPa]	[MPa]	[GPa]	[mm]	[-]	[g/m^2]	[mm]	[MPa]	[GPa]	[%]	[-]	[°]	[-]	[MPa]	[MPa]	[-]	
[15]	E7#2-1,..3	3	150	2.0				10		4.72[3]	0.254	2800	190.00	1.50	2		0.66		45.21	–	JF
	E9#1-1,..3	3	150	2.0	55.00	10.00	25.00	7	UD	4.72[3]	0.254	2800	190.00	1.50	1	90	0.32	29.98	45.87	–	*D*
	E10#2-1,..3	3	150	2.0				10		4.72[3]	0.254	2800	190.00	1.50	2		0.64		64.19	–	*JF-D*

Notes: * preimpregnated with resin; ** preimpregnated with latex; *** mesh coated with "modified acrylic polymer"; [1] elastic modulus expressed in [kN/m] (per unit width); [2] weight without coating; [3] density expressed in [cord/cm]; [4] jacket applied onto a wax-based bond breaker to facilitate removal, aiming at ensuring reversibility.
Source: [1] Di Ludovico et al. 2010; [2] García et al. 2010; [3] Sadrmomtazi et al. 2016; [4] Al-Gemeel & Yan Zhuge 2019; [5] Triantafillou et al. 2006; [6] Ortlepp et al. 2011; [7] Colajanni et al. 2014; [8] Zeng et al. 2017; [9] Gonzalez-Libreros et al. 2018; [10] Donnini et al. 2019; [11] Libreros et al. 2019; [12] Gopinath et al. 2011; [13] De Caso y Basalo et al. 2012; [14] Bhuvaneshwari et al. 2014; [14] Trapko 2013; [15] Ombres 2014; [16] Ombres 2017; [17] Thermou et al. 2016; [18] Thermou & Hajirasouliha 2018.

In regard to the failure mode experienced by the FRCM confined specimens, it is worth to highlighting that, as mentioned earlier, the compressive behavior of the FRCM-confined concrete is significantly influenced by the cracking of the inorganic matrix. Depending on cracking severity, two main failure modes can be observed: *a)* tensile failure of the external jacket in the hoop direction (JF) and, *b)* jacket opening, i.e., debonding of the confining system (D). In most cases, mortar cracking was observed with the opening of vertical cracks in the overlapping zones and their more or less slow and symmetric propagation along the jacketed cylinder surface. Of course, the greater or lesser width of these cracks has an effect on the slip activated at the fiber-matrix interface, so that either a debonding-induced failure within the matrix or a jacket failure occurs. To this aim, the bar chart in Figure 3 shows, for each FRCM system, the percentage distribution of the specimens' datasets which failed by jacket failure or debonding (the datasets number is in the white square of each bar).

Based on the collected data, the Figure shows that the debonding failure was rather common for the cases of G-FRCM, S-FRCM and C-FRCM systems (probability of occurrence also over 30%) whereas it was missing for PBO-FRCM confined specimens. However, looking at the data collected in the database, it was not found, at this stage, a clear correlation between the observed failure mode and any of the parameters collected in Table 1, particularly the strength and the thickness of the employed mortar, or the thickness and the number of fabric layers. This aspect will deserve, of course, more investigation in the next studies.

2.1 Strain efficiency of the FRCM system

It has been already shown for the case of FRP composites that the hoop strain of the confining system measured at collapse ($\varepsilon_{j,u}$) is typically lower than the ultimate strain found from flat coupon tensile tests ($\varepsilon_{f,u}$), that means k_ε<1. In literature, different values of k_ε have been suggested for the case of carbon and glass FRP systems, typically ranging between 0.5 and 0.7.

The several reasons of the reduced FRP efficiency are summarized in a previous paper published by the authors (Realfonzo and Napoli 2011); among them, the accuracy used in measuring the experimental hoop strains (generally with strain gauges or LVDTs) is, of course, a key parameter.

However, having reliable measures of the hoop strains in the case of confinement by FRCM system is quite difficult since the experimental reading of strains could soon fail because of the mortar cracking. To address this issue in some way, strain gauges should be arranged directly on the fabric before mortar application but, at the same time, assuring a correct installation is not easy, especially on BD fabrics, lacking fiber continuity. For these reasons, very few data on the k_ε factor were gathered in the database and only for B-FRCM, G-FRCM and PBO-FRCM systems for which the following average values of k_ε were respectively calculated from a certain number of datasets: 0.27 (n = 4), 0.22 (n = 7) and 0.47 (n = 31); no data is available for C-FRCM and S-FRCM systems.

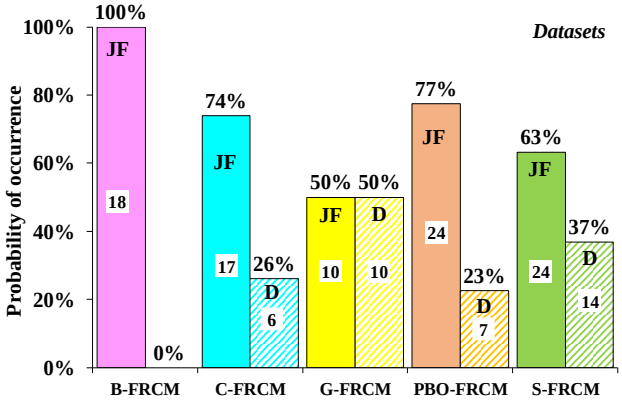

Figure 3. Failure mode: % distribution of datasets.

3 BEST-FIT ANALYSES

Based on the collected database, preliminary models for predicting the strength of the FRCM-confined concrete with circular cross-section, f_{cc}, were developed through best-fit analyses.

The models were formulated in a non-dimensional form by means of the following equation specified for circular sections:

$$\bar{f}_{cc} = \frac{f_{cc}}{f_{c0}} = 1 + \alpha \cdot \bar{f}_l^{\beta} \quad (3)$$

which is that generally accepted for the FRPs.

Of course, based on the earlier considerations on the role of the inorganic matrices, the application of Eq. (3) to FRCM systems is an important simplification of the real behavior. On the other hand, as long as the mechanical properties of the inorganic matrices are not – or not exhaustively - documented in the literature, the above mentioned approximation is necessary.

In Eq. (3), α and β are two unknown parameters to be calibrated through best-fit techniques aimed at minimizing the difference between the predicted and the experimental values of the strength, whereas $\bar{f}_l$ is the normalized confining pressure exerted by the FRCM jacket, expressed by Eq. (1).

Table 3 reports the results of the best-fit analyses performed to find the values of the parameters α and β which minimize the mean error $(E_{rr})_m$ between the experimental data $\bar{f}_{cc}^{exp}$ and the theoretical one $\bar{f}_{cc}^{th}$. The error minimization on the *n* datasets has been performed by applying both the mean absolute percentage error (MAPE) and the mean square error (MSE) methods, respectively expressed by:

$$(E_{rr})_m^{MAPE} = \frac{\sum_{i=1}^{n}|E_i|}{n};\ E_i = \frac{\left(\bar{f}_{cc,i}^{exp} - \bar{f}_{cc,i}^{th}\right)}{\bar{f}_{cc,i}^{exp}} \cdot 100 \quad (4a)$$

$$(E_{rr})_m^{MSE} = \frac{\sum_{i=1}^{n} E_i}{n};\ E_i = \left(\bar{f}_{cc,i}^{exp} - \bar{f}_{cc,i}^{th}\right)^2 \quad (4b)$$

The analyses were, in a first step, carried out only by considering the datasets included in "JF" failure mode ("JF" case) and, then, on all the datasets, irrespectively of the failure mode ("JF+D" case). Since the best-fit analyses did not show significant differences between two examined cases, the results in Table 3 are related to the "JF+D" case.

It is noted that the number n in Table 3 does not always coincide with the total one available for each FRCM system, since some datasets were excluded in the analyses due to the lack of proper information or uncertainty in the available tests.

Also, as known for the FRP systems, the analyses were performed by considering all datasets for which the lateral confining pressure $\bar{f}_l$ (see Eq. 1) was greater than 7% in order to consider a *"sufficiently confined concrete"* (Realfonzo and Napoli 2011). An exception is represented by the analyses carried out for the B-FRCM system for which, due to the limited number of datasets characterized by rather high values of $\bar{f}_l$, the threshold was lowered to 6%.

The best-fit analyses were carried out on datasets belonging to the single type of FRCM system by considering the following cases:

- *case a)* α ≠1 & β=1 (Model 1, i.e., linear model),
- *case b)* α≠1 & β ≠1 (Model 2, i.e., nonlinear model).

Table 3. Results of the best-fit analyses.

FRCM System	N	n	k_ε	Model	MAPE			MSE		
					α	β	$(Err)_m$	α	β	$(Err)_m$
B-FRCM	49	12	1.00	1	3.19	1.00	10.67%	2.46	1.00	3.69%
				2	-	-	-	-	-	-
			0.27	1	12.05	1.00	10.67%	9.30	1.00	3.69%
				2	-	-	-	-	-	-
C-FRCM	46	21	1.00	1	0.99	1.00	8.84%	0.95	1.00	3.41%
				2	0.55	0.50	7.87%	0.66	0.52	2.51%
G-FRCM	45	15	1.00	1	0.42	1.00	11.12%	0.45	1.00	4.17%
				2	0.50	0.78	10.00%	0.54	0.64	3.53%
			0.22	1	1.95	1.00	11.12%	2.07	1.00	4.17%
				2	1.68	0.79	10.08%	1.43	0.64	3.53%
PBO-FRCM	40	29	1.00	1	1.22	1.00	15.13%	1.76	1.00	8.99%
				2	1.22	1.00	15.13%	1.76	1.00	8.99%
			0.47	1	2.19	1.00	16.95%	3.16	1.00	11.15%
				2	2.19	1.00	16.95%	3.16	1.00	11.15%
S-FRCM	73	34	1.00	1	2.61	1.00	13.64%	2.08	1.00	8.17%
				2	1.45	0.55	7.93%	1.50	0.56	3.90%

Due to the lack of a sufficient amount of information for the strain efficient factor k_ε, the analyses were first performed by considering k_ε = 1 in Eq. (1) for all the FRCM systems. Then, for the case of B-FRCM, G-FRCM and PBO-FRCM systems, the analyses were also performed by considering the respective average values of k_ε obtained from the experimental data; the results of these analyses for both MAPE and MSE methods are in grey background in Table 3.

Figures 4a,c,e,g, 5a,c,e,g, and 6a,c, show the comparison between the found best-fit models and the experimental data where the $\bar{f}_l$ values were calculated by plugging k_ε = 1 in Eq. (1).

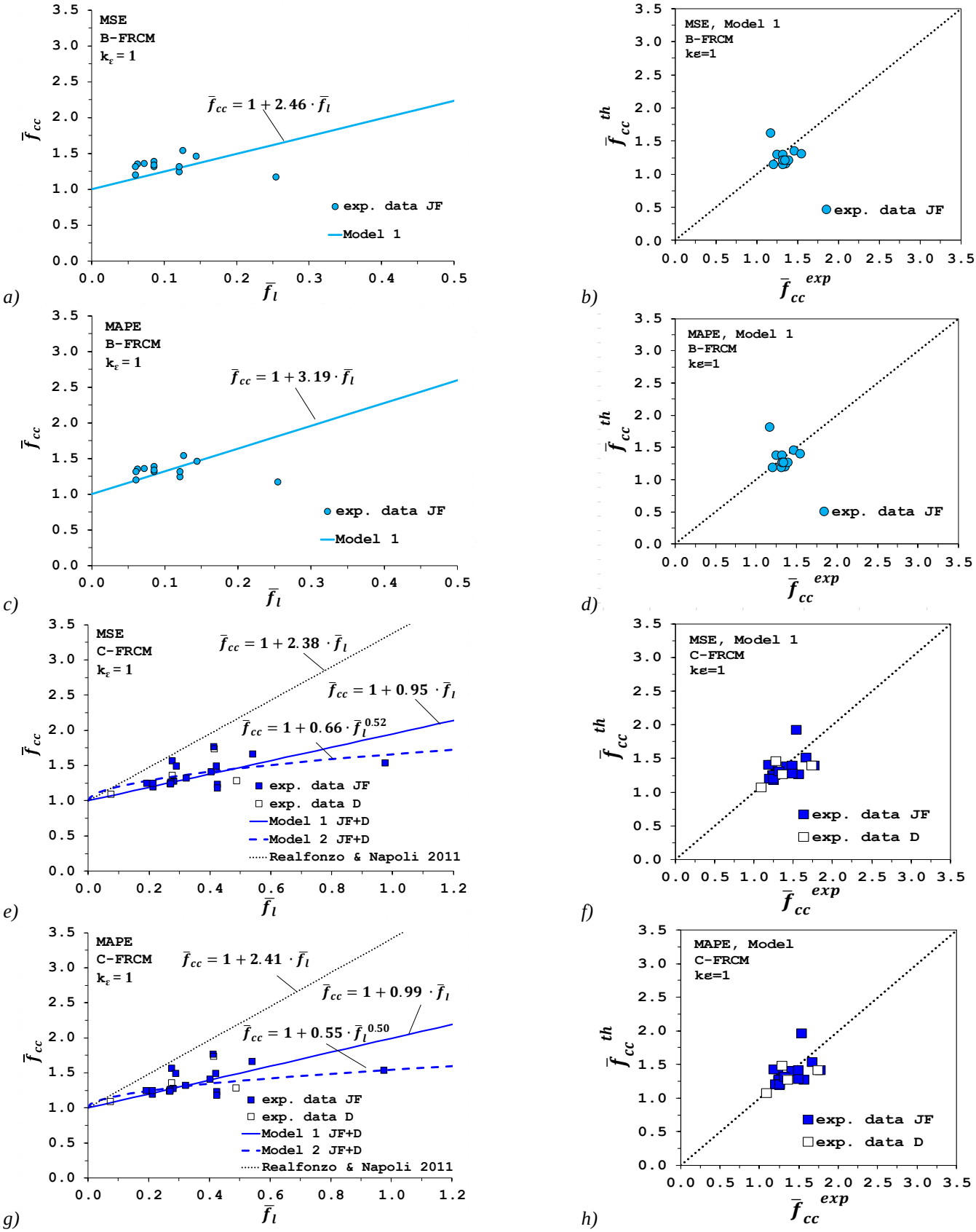

Figure 4. Predictive models and their accuracy for: B-FRCM (a,b,c,d) and C-FRCM system (e,f,g,h).

For the C-FRCM (Fig. 4e,g), G-FRCM (Fig. 5a,c) and S-FRCM (Fig. 6a,c) systems, the theoretical formulae proposed by Realfonzo and Napoli (2011) and Napoli and Realfonzo (2016) for the corresponding C-, G-FRP and S-FRP systems (in the case of $k_\varepsilon = 1$), are also plotted for comparison.

Furthermore, in order to better investigate the efficacy of the found strength models, in Figures 4b,d,f,h, 5b,d,f,h and 6b,d the theoretical values $\bar{f}_{cc}^{th}$ calculated for each dataset were compared with the experimental ones $\bar{f}_{cc}^{exp}$.

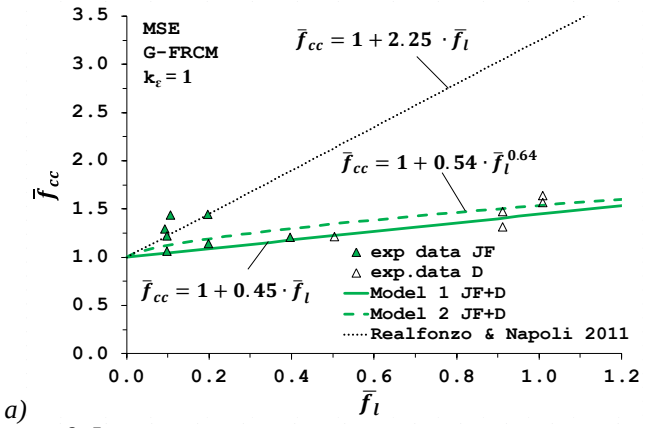

a)

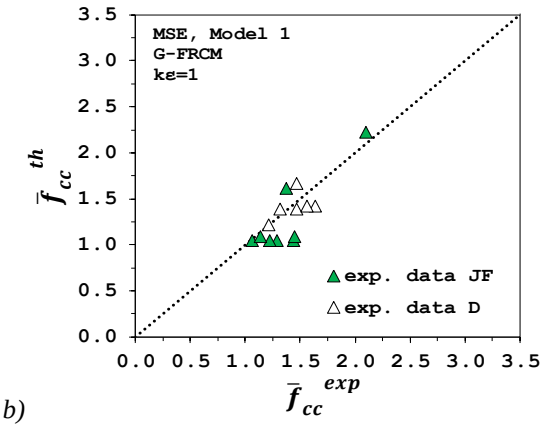

b)

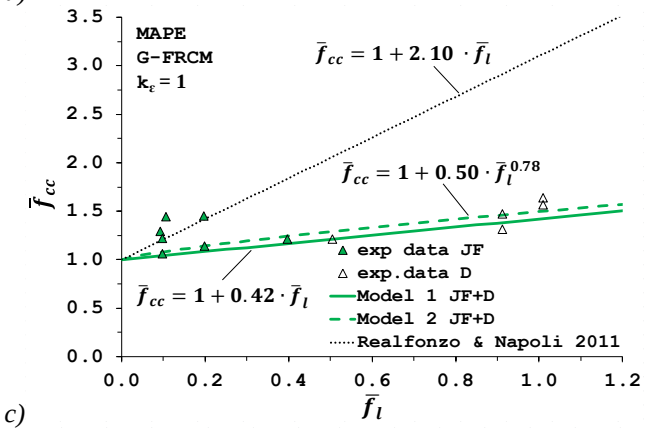

c)

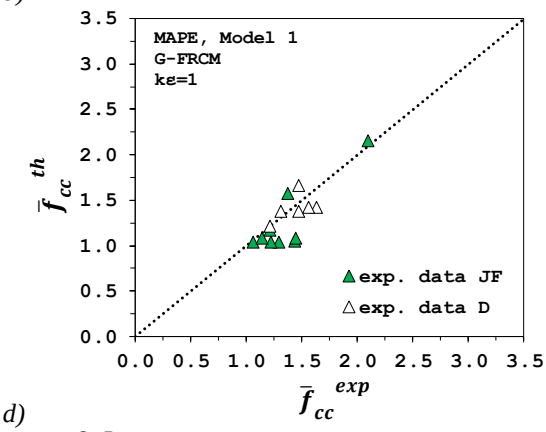

d)

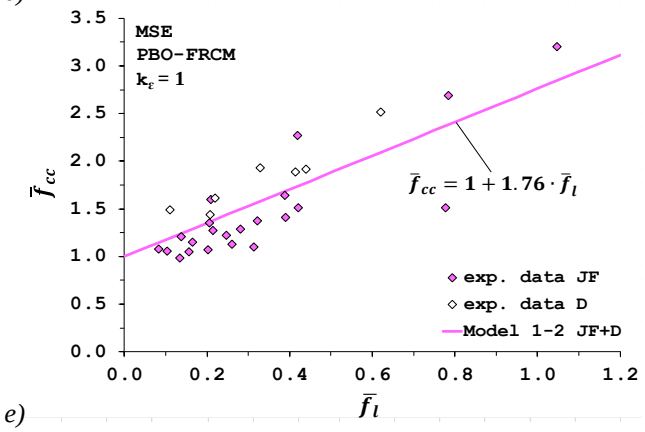

e)

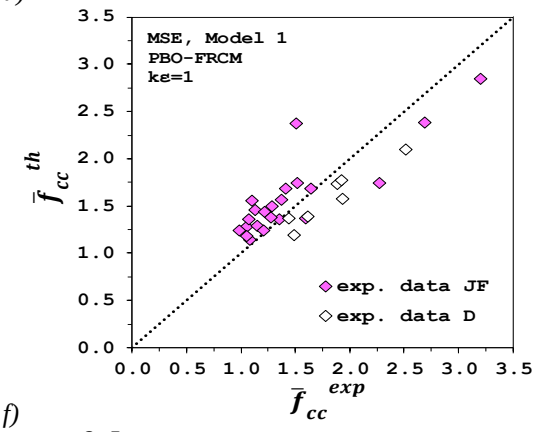

f)

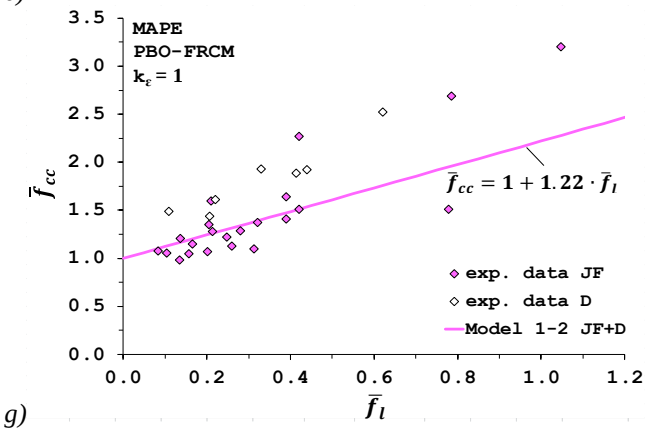

g)

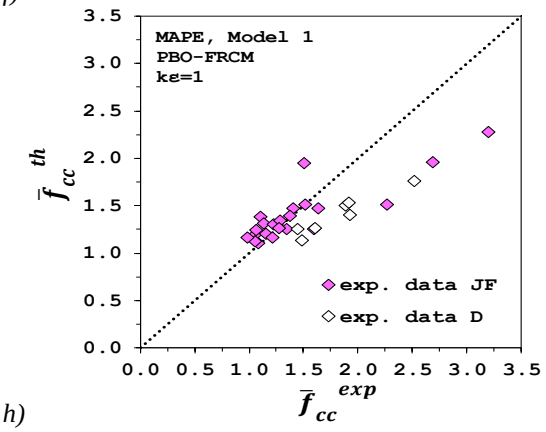

h)

Figure 5. Predictive models and their accuracy for: G-FRCM (a-d) and PBO-FRCM system (e-h).

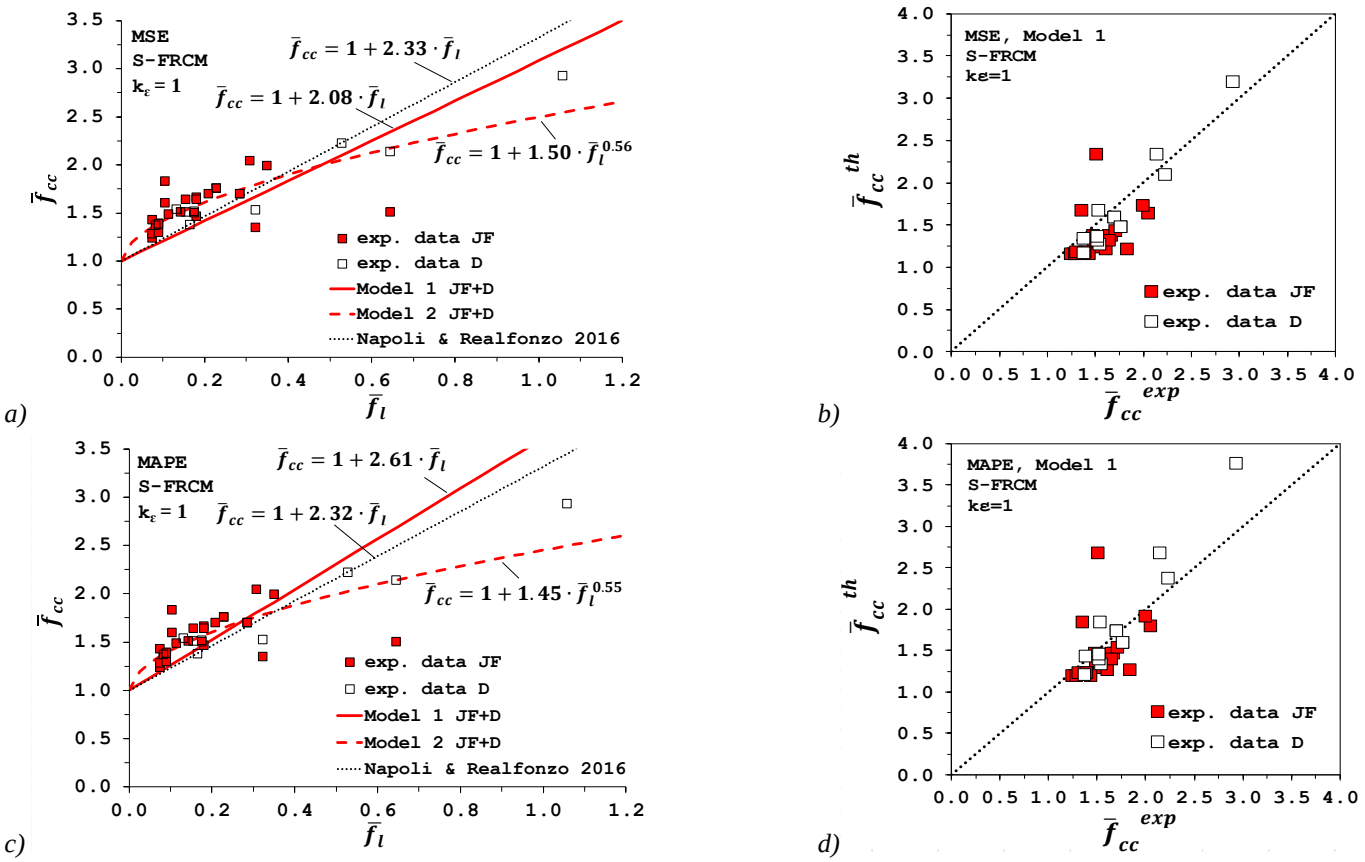

Figure 6. Predictive models and their accuracy for: S-FRCM system (a-d).

The bisector corresponds to perfect agreement between prediction and tests; therefore, points falling in the lower part of the graph indicate conservative predictions whereas points falling over the line represent unconservative situations.

Finally, in Figure 7 all the linear best-fit curves (i.e., Model 1 in Table 3) obtained by using the MSE (Fig. 7a) and MAPE (Figure 7b) method are plotted together.

The results of the performed best-fit analyses in Figure 4-7 show that, for any given value of $\bar{f}_l$, the lowest strength is obtained in the case of G- and C-FRCM systems, whatever the fitting method used (MSE or MAPE). The fairly unsatisfactory results yielded by these two systems is confirmed by comparing the best-fit models with the relationships found by Realfonzo and Napoli (2011) for glass and carbon FRP systems (Fig.4e,g and Fig.5a,c).

Conversely, the best performance is exhibited by PBO- and S-FRCM systems. In particular, in the latter case the relationships are very similar to those published in Napoli and Realfonzo (2016) for steel FRP composites. This result, even though based on a limited amount of experimental data, seems to highlight that the use of inorganic matrices in combination with steel fibers, does not produce a significant reduction of the confinement efficiency with respect to epoxy matrices (as observed, instead, in the case of carbon and glass fibers).

Whatever the fitting method used (MSE or MAPE), the lowest and highest errors were always obtained in the case of the C-FRCM and PBO-FRCM system, respectively. However, in all the cases a good agreement between predictions and experimental data can be observed in the plots of Figure 4b,d,f,h, 5b,d,f,h and 6b,d, with estimates generally more conservative by using the MSE method.

Except for the PBO-FRCM system, the nonlinear relationships (see the results for the Model 2 in Table 3) are those fitting the experimental data better. However, in the $\bar{f}_l$ range of interest (lower than 0.5-0.6) the two considered models are very similar.

Finally, by looking at Figure 7, it is observed that, for the case of the MAPE method, the linear relationships obtained for C- and PBO-FRCM systems are very similar and, therefore, a unique model might be used to predict the strength performance of both composites. This similarity is not observed for the case of the MSE method where the law obtained for the PBO-FRCM system becomes rather similar to those of the steel and basalt fibers.

Figure 8 shows, for the case of B-FRCM (Fig. 8a,b), G-FRCM (Fig.8c,d) and G-FRCM (Fig.8e,f), the comparison between the experimental data and the linear best-fit models obtained by considering $k_\varepsilon \neq 1$ in the estimate of the lateral confining pressure.

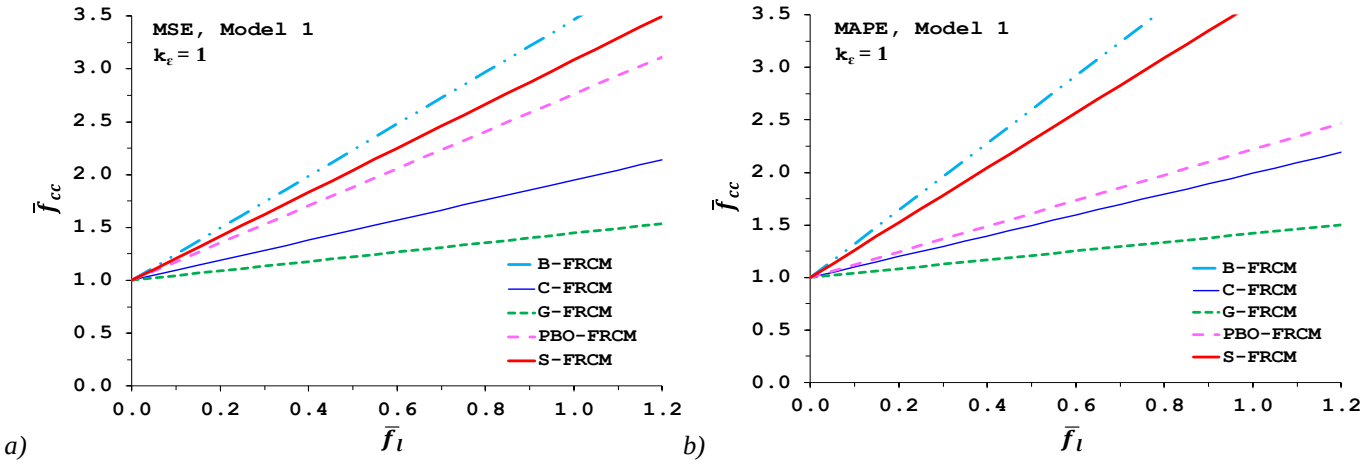

Figure 7. Summary of the best-fit models obtained with MSE (a) and MAPE method.

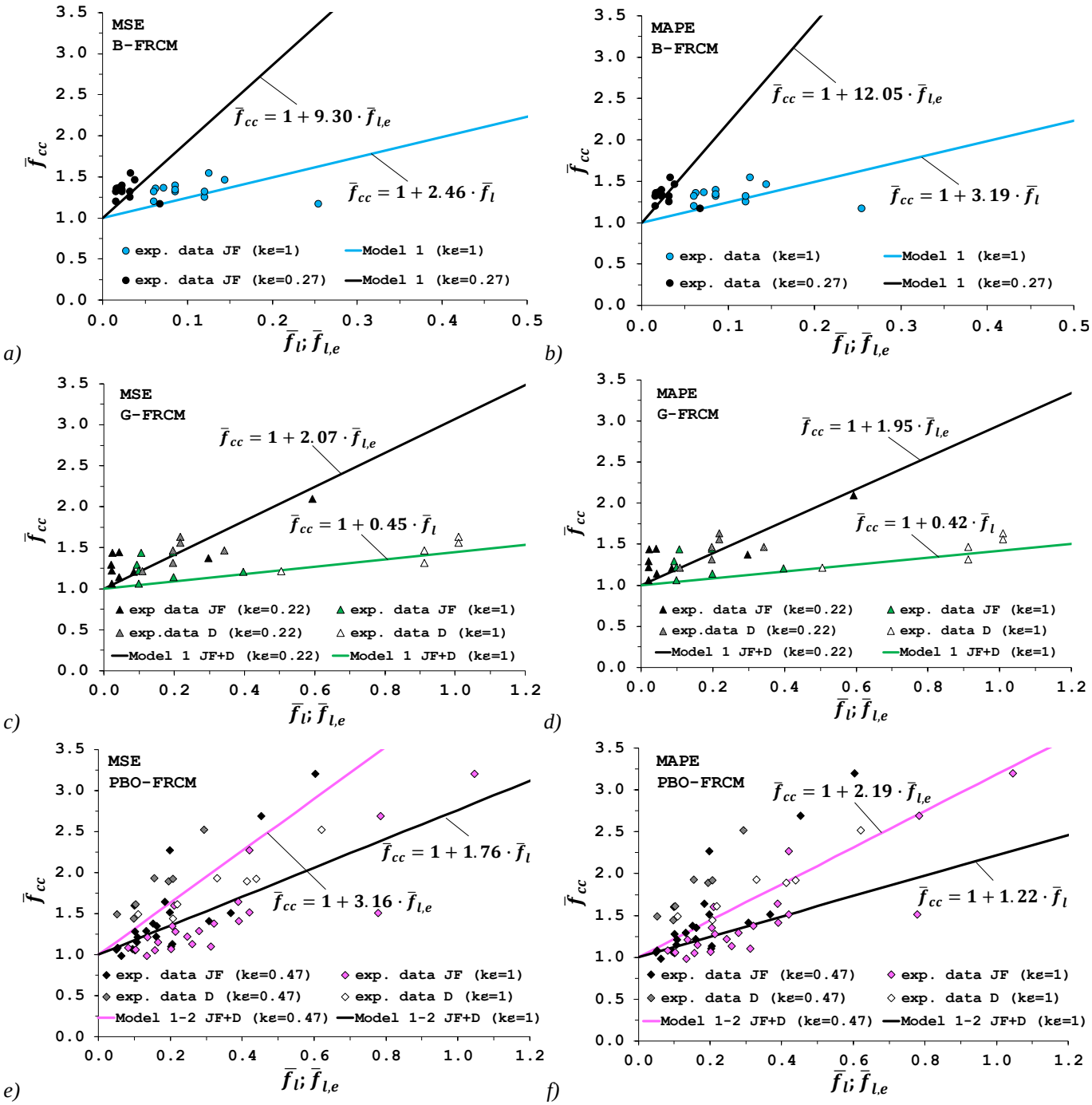

Figure 8. Predictive models for B-FRCM (a,c), G-FRCM (c,d) and PBO-FRCM (e,f) systems in the case of $k_\varepsilon \neq 1$.

In particular, the average value of k_ε found from a limited number of datasets available for each of the three considered systems was extended to all datasets, and new best-fit analyses were performed by considering the effective lateral confining pressure $f_{l,e}$ ($k_\varepsilon \neq 1$) instead of the ultimate ones f_l .

Even though more investigation is needed, the results in Figure 8 highlight a significant reduction of the confinement efficiency for the B- and G-FRCM systems, so that the slope of the linear relationships have to increase of about 4 times in order to fit the experimental data well (the k_ε values for these two systems are well below the unit).

Conversely, the value of k_ε obtained for the PBO-FRCM system ($k_\varepsilon = 0.47$) is rather similar to the values found in literature for the case of FRPs (Realfonzo and Napoli 2011; Napoli and Realfonzo 2016).

4 COMPARISONS WITH EXISTING FORMULAE

As mentioned earlier, the best-fit models discussed in Section 3 have been developed, as a first attempt, by neglecting the contribute of the inorganic matrix which can have influence on the strength performance. However, this approach was preferred in this stage, mainly because of the uncertainty related to: *a)* the mechanical properties of the matrix types used in the experimental tests (sometimes not provided in the scientific papers), and *b)* the characteristics directly correlated to the FRCM application, such as the thickness of the mortar layer used in the test specimens (information sometimes missing in the scientific papers).

However, by using their own experimental database, Cascardi et al. (2017) proposed an analytical model for the prediction of the strength performance of any FRCM system which accounts for the influence of the inorganic matrix through the parameter k, given by:

$$k = 4 \cdot \rho_m \frac{f_{m,c}}{f_{c0}};\ \rho_m = \frac{4 \cdot t_m}{D} \tag{5}$$

From Eq. (5) it is noted that k depends on both the ratio between the compressive strength of the mortar ($f_{m,c}$) and that of the unconfined concrete (f_{c0}) and the parameter ρ_m, defined as the geometrical percentage of the applied matrix in the FRCM system. The latter, in turn, depends on thickness of the mortar layer employed for the FRCM application (t_m) and the diameter of the circular cross-section of the column (D).

Therefore, the strength model proposed by Cascardi et al. (2017), normalized with respect to $f_{c0,}$ is expressed by:

$$\bar{f}_{cc} = 1 + k \cdot \bar{f}_l \tag{6}$$

with the lateral confining pressure given by:

$$\bar{f}_l = \frac{t_f \cdot n_f \cdot E_f \cdot \varepsilon_{f,u}}{D} \tag{7}$$

Lately, the recently published document CNR-DT 215 (2018) suggested to use the following formula for predicting the strength of concrete confined with FRCM, which is here written without safety factors:

$$\bar{f}_{cc} = 1 + 2.6 \cdot \bar{f}_{l,e}^{\,2/3} \tag{8}$$

where the effective lateral confining pressure $\bar{f}_{l,e}$ is given by:

$$\bar{f}_{l,e} = \frac{2 \cdot t_f \cdot n_f \cdot E_f \cdot \varepsilon_{f,e}}{D} \tag{9}$$

In Eq. (9), the effective strain of the FRCM jacket ($\varepsilon_{f,e}$) is estimated as follows:

$$\varepsilon_{f,e} = min\left(k_m \cdot \varepsilon_{f,u}; 0.004\right) \tag{10a}$$

$$k_m = 0.217 \cdot \left(\rho_m \frac{f_{m,c}}{f_{c0}}\right)^{3/2} \leq 1 \tag{10b}$$

In order to compare the accuracy of the above mentioned formulae with that of the simplified relationships proposed in Section 3 (i.e. Model 1 and Model 2), Table 4 provides the model errors calculated with both MSE and MAPE for each of the FRCM system. Figure 9, instead, depicts the comparison between the experimental values and the theoretical predictions in terms of $\bar{f}_{cc}$, obtained by applying the two mentioned models.

Table 4. Comparison among strength models.

FRCM	Cascardi et al. (2017)		CNR-DT 215 (2018)		Model 1		Model 2	
System	MSE	MAPE	MSE	MAPE	MSE	MAPE	MSE	MAPE
B-FRCM	1.64%	8.71%	6.72%	17.98%	3.69%	10.67%	-	-
C-FRCM	32.18%	29.81%	3.35%	11.27%	4.17%	11.12%	3.53%	10.00%
G-FRCM	45.69%	33.14%	13.01%	20.14%	3.41%	8.84%	2.51%	7.87%
PBO-FRCM	40.66%	23.94%	30.34%	19.26%	8.99%	15.13%	8.99%	15.13%
S-FRCM	12.06%	19.55%	29.17%	29.52%	8.17%	13.64%	3.90%	7.93%

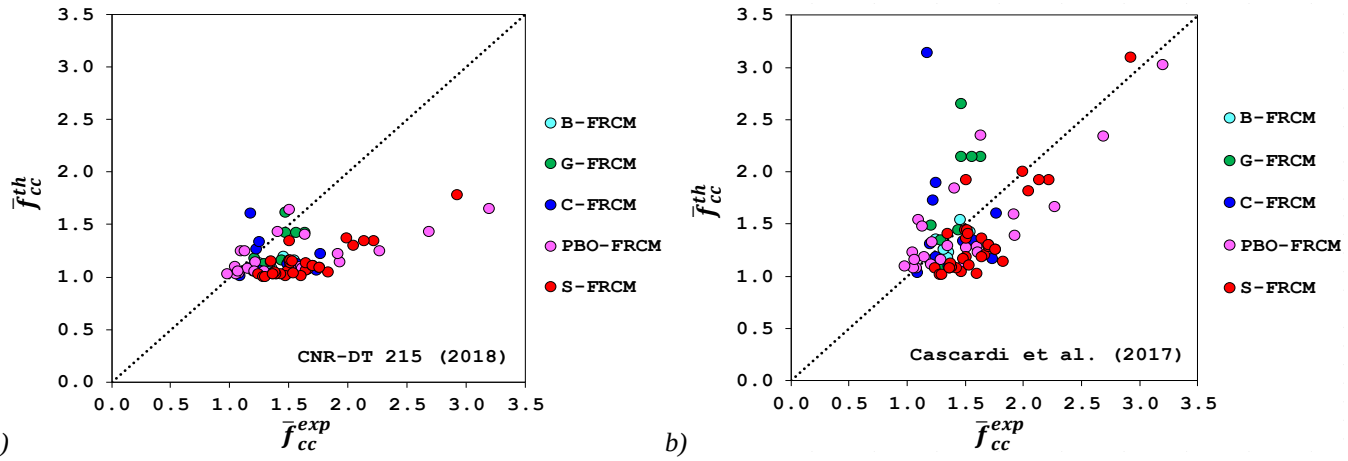

a) *b)*

Figure 9. Accuracy of strength models according to: (a) CNR-DT 2015 (2018); (b) Cascardi et al. (2017)

As shown, the relationship by Cascardi et al. fits the experimental data very well in the case of the B-FRCM system (even better of the Model 1) and provides good predictions also for the S-FRCM system. Conversely, based on the available data, it seems to be less accurate for carbon, glass and PBO fibers.

The relationship by CNR-DT 215 (2018), instead, is less effective for basalt and steel fibers and works better for the other ones.

However, by looking at Figure 9, it seems that the model by CNR-DT 215 (2018) generally provides too much conservative predictions, with several data falling below the 45° bisector and distributed very far from this line. This is a relevant aspect to consider since, for design purposes, the document suggests to apply some safety factors to the strength model which further decrease the contribute of the external confinement.

Overall, it can be observed that the simplified Model 1 and Model 2, even though they do not account for the influence of the mortar, yield good predictions in comparison to the counterpart models, with errors do not overcoming 9% and 16% for the case of the MSE and MAPE, respectively.

Of course, the study presented herein will deserve more investigation in the near term in order to better check, on one side, the reliability of the proposed simplified models on the basis of more experimental data and, on the other side, the effective importance of considering the contribute of the mortar in the strength formulae.

5 CONCLUSIONS

A number of models aimed at predicting the compressive strength of concrete laterally confined with Fabric-Reinforced Cementitious Matrices – FRCMs is presented in this preliminary study. Model calibration is performed by applying best-fit techniques to the experimental results collected in a wide database, which allows each FRCM system (containing glass, carbon, steel or polybenzobisoxazole fabrics) to be treated separately. The analyses show that the lowest strength is exhibited by the systems containing glass or carbon fabrics, whatever the best-fit method be used. Conversely, the best performance is exhibited by the systems containing PolyBenzobisOxazole - PBO or steel fabrics. In the case of steel fabrics, the formulae for the evaluation of the strength of the composite are similar to those developed in the case of steel fiber-reinforced polymers - SFRPs.

The proposed models, even though they do not account for the influence of the mortar, yield good predictions when compared to the analytical formulations accounting for the contribute of the inorganic matrix. However, further research is needed to better investigate the reliability of the proposed models on the basis of a larger experimental database and check the effective importance of considering the contribute of the mortar in the analytical formulae.

ACKNOWLEDGEMENTS

The study has been financially supported by ReLUIS-Italian Department of Civil Protection's Executive Project 2019-21 (WP14).

REFERENCES

Al-Gemeel, A.N., Zhuge Y., 2019. Using textile reinforced engineered cementitious composite for concrete columns confinement. *Composite Structures*, **210**, 695–706.

Ascione, L., de Felice, G., De Santis, S., 2015. A qualification method for externally bonded Fibre Reinforced Cementitious Matrix (FRCM) strengthening systems. *Composites Part B: Engineering*, **78**, 497–506.

Bhuvaneshwari, P., Saravana Raja Mohan, K., Kirthiga, R., 2014. Stress strain behaviour of concrete element retrofitted using organic and inorganic binders. *Asian Journal of Applied Sciences*, **7**(4), 215–223.

Carloni, C., Bournas, D.A., Carozzi, F.C., D'Antino, T., Fava, G., et. al., 2016. Fiber Reinforced Composites with Cementitious (Inorganic) Matrix. In: *AA.VV. Design Procedures for the Use of Composites in Strengthening of Reinforced Concrete Structures- State-of-the-Art Report of the RILEM Technical Committee 234-DUC*, 349-392, Springer.

Carloni, C., Ascione, F., Camata, G., De Felice, G., De Santis, S., Lamberti, M., Napoli, A., Realfonzo, R., Santandrea, M., Stievanin, E., Cescatti, E., Valluzzi, M.R., 2018. An overview of the design approach to strengthen existing reinforced concrete structures with SRG. *ACI Special Publication* (SP 326).

Cascardi, A., Longo, F., Micelli, F., Aiello, M.A., 2017. Compressive strength of confined column with Fiber Reinforced Mortar (FRM): New design-oriented-models. *Construction and Building Materials*, **156**, 387–401.

Colajanni, P., Fossetti, M., Macaluso, G., 2014. Effects of confinement level, cross-section shape and corner radius on the cyclic behavior of CFRCM confined concrete columns. *Construction and Building Materials*, **55**, 379–389.

D'Ambrisi, A., Feo, L., Focacci, F., 2013. Experimental and analytical investigation on bond between Carbon-FRCM materials and masonry. *Composites Part B: Engineering*, **46**, 15–20.

De Caso y Basalo, F.J., Matta, F., Nanni, A., 2012. Fiber reinforced cement-based composite system for concrete confinement. *Construction and Building Materials*, **32**, 55–65.

Di Ludovico, M., Prota, A., Manfredi, G. 2010. Structural upgrade using basalt fibers for concrete confinement. *J. of Composites for Construction*, **14**(5), 541-552.

Donnini, J., Spagnuolo, S., Corinaldesi, V., 2019. A comparison between the use of FRP, FRCM and HPM for concrete confinement. *Composites Part B*: Engineering, **160**, 586–594.

Faella, C., Monaco, V., Napoli, A., Realfonzo, R., 2018. Confinement of concrete with FRCM materials. *Proceedings of Italian Concrete Days*, Lecco, 1-8.

García, D., Alonso, P., San-José, J.T., Garmendia, L., Perlot, C., 2010. Confinement of medium strength concrete cylinders with basalt textile reinforced mortar. *Proc. of the 13th Int. Congress on Polymers in Concrete*, ICPIC 2010, Madeira, Portugal.

Gonzalez-Libreros, J., Sabau, C., Sneed, L.H., Sas, G., Pellegrino, C., 2018. Effect of Confinement with FRCM Composites on Damaged Concrete Cylinders. *RILEM Bookseries*, **15**, 770–777.

Gopinath, S., Iyer, N.R., Gettu, R., Palani, G.S., Ramachandra Murthy, A., 2011. Confinement effect of glass fabrics bonded with cementitious and organic binders. *Procedia Engineering*, **14**, 535–542.

Italian National Research Council (CNR), 2013. Guide for the design and construction of externally bonded FRP systems for strengthening existing structures. *CNR-DT200 R1*, Rome.

Italian National Research Council (CNR), 2018. Istruzioni per la Progettazione, l'Esecuzione ed il Controllo di Interventi di Consolidamento Statico mediante l'utilizzo di Compositi Fibrorinforzati a matrice inorganica. *CNR-DT 215/2018*, Rome.

Napoli, A., Realfonzo, R., 2016. Compressive behavior of concrete confined by SRP wraps. *Construction and Building Materials*, **127**, 993-1008.

Ombres, L., 2014. Concrete confinement with a cement based high strength composite material. *Composite Structures*, **109**, 294–304.

Ombres, L., Mazzuca, S., 2017. Confined Concrete Elements with Cement-Based Composites: Confinement Effectiveness and Prediction Models. *J. of Composite for Construction*, **21**(3), 1–15.

Ombres, L., 2017. Structural performances of thermally conditioned PBO FRCM confined concrete cylinders. *Composite Structures*, **176**, 1096–1106.

Ortlepp, R., Lorenz, A., Curbach, M., 2011. Geometry effects onto the load bearing capacity of column heads strengthened with TRC. *Proc. of fib Symp.*, Prague, Czech Republic.

Realfonzo, R., Napoli, A., 2011. Concrete confined by FRP systems: Confinement efficiency and design strength models. *Composites Part B: Engineering*, **42**(4), 736–755.

Sadrmomtazi, A., Khabaznia, M., Tahmouresi, B., 2016. Effect of Organic and Inorganic Matrix on the Behavior of FRP-Wrapped Concrete Cylinders. *Journal of Rehabilitation in Civil Engineering*, **4**(2), 52–66.

Thermou, G.E., Katakalos, K., Manos, G., 2016. Influence of the cross section shape on the behavior of SRG-confined prismatic concrete specimens. *Materials and Structures*, **49**, 869–887.

Thermou, G.E., Hajirasouliha, I., 2018. Compressive behaviour of concrete columns confined with steel-reinforced grout jackets. *Composites Part B: Eng*ineering, **138**, 222–231.

Trapko, T., 2013. Fibre Reinforced Cementitious Matrix confined concrete elements. *Materials and Design*, **44**, 382–391.

Triantafillou, T.C., Papanicolaou, C.G., Zissimopoulos, P., Laourdekis, T., 2006. Concrete Confinement with Textile-Reinforced Mortar Jackets. *ACI Structural J.*, **103**(1), 28–37.

Zeng, L., Li, L.J., Liu, F., 2017. Experimental Study on Fibre-Reinforced Cementitious Matrix Confined Concrete Columns under Axial Compression. *Kem. Ind.*, **66**(3-4), 165–172.